Commun. Theor. Phys. **76** (2024) 075702 (11pp) https://doi.org/10.1088/1572-9494/ad3955

# Existence of long-range magnetic order in Heisenberg spin nanoribbons with edge modification

**Da-cheng Ma[1], Ling-yi Cui[1], Chu-xiao Sun[1], Xiao-dan Chi[2], Zheng-Nan XianYu[3] and An Du[1,4,5,6]**

[1] College of Science, Northeastern University, Shenyang 110819, China
[2] Department of Basic Science, Dalian Naval Academy, Dalian 116018, China
[3] Department of Physics, College of Sciences, Shenyang University of Chemical Technology, Shenyang 110142, China
[4] National Frontiers Science Center for Industrial Intelligence and Systems Optimization, Northeastern University, China
[5] Key Laboratory of Data Analytics and Optimization for Smart Industry (Northeastern University), Ministry of Education, China

E-mail: duan@mail.neu.edu.cn

Received 24 January 2024, revised 1 April 2024
Accepted for publication 2 April 2024
Published 3 June 2024

**Abstract**

Long-range magnetic order appears on a side decorated Heisenberg spin nanoribbon at nonzero temperature, although no spontaneous magnetization exists in a one- or two-dimensional isotropic Heisenberg model at any nonzero temperature according to the Mermin–Wagner theorem. By use of the spin Green's function method, we calculated the magnetizations of Heisenberg nanoribbons decorated by side spins with single-ion anisotropy and found that the system exhibits a nonzero transition temperature, whether the decorated edge spins of the system link together or separate from each other. When the width of the nanoribbon achieves infinite limit, the transition temperatures of the system tend to the same finite constant eventually whether one edge or both edges are decorated by side spins in the nanoribbon. The results reveal that the magnetism of a low-dimensional spin system is different from that of a three-dimensional spin system. When the single-ion anisotropy of edge spins in a Heisenberg spin nanoribbon can be modulated by an electric field experimentally, various useful long-range magnetic orders of the system can be obtained. This work can provide a detailed theoretical basis for designing and fabricating next-generation low-dimensional magnetic random-access memory.

Supplementary material for this article is available online

Keywords: Nanoribbon, magnetic anisotropy, long-range magnetic order, Heisenberg model, transition temperature

## 1. Introduction

For the past few years, two-dimensional (2D) van der Waals crystals have usually been regarded as an important arena for studying 2D magnetism [1–14]. Due to the development of the exfoliation method and various other methods [15–17], the thickness of 2D magnetic materials can be precisely controlled experimentally, and these layered 2D materials exhibit novel properties different from those of the three-dimensional system [18–27]. For example, $CrI_3$ bilayers with small twist angle exist with both ferromagnetic and anti-ferromagnetic ground states [28–30]. The spin prefers an in-plane direction in 2D room-temperature ferromagnetic 1T-$CrTe_2$ [31–34]. Monolayer $Fe_3GeTe_2$ and $Fe_3GaTe_2$

[6] Author to whom any correspondence should be addressed.

exhibit robust intrinsic 2D ferromagnetism with strong perpendicular anisotropy [35, 36]. Using scanning magneto-optic Kerr microscopy, an unexpected intrinsic long-range ferromagnetic order is found in pristine layered $Cr_2Ge_2Te_6$ [3]. At room temperature, 2H-phase vanadium diselenide ($VSe_2$) shows magnetic order in the 2D form only, in which the 3d orbitals of $V^{4+}$ ions split into different groups due to structural anisotropy [37]. An exceptionally sizable orbital moment of the $V^{3+}$ ion is displayed in the $VI_3$ monolayer [38]. The physical mechanism of intrinsic 2D magnetism remains elusive, although many novel and unique magnetic phenomena have been discovered experimentally.

The Mermin–Wagner–Hohenberg theorem proves that there is no long-range magnetic order at any nonzero temperature for a one- or two-dimensional isotropic Heisenberg model (meaning the long-range magnetic order is destroyed by thermal fluctuations), however, magnetic anisotropy can suppress the effect of thermal fluctuations [39, 40]. It is obvious that magnetic anisotropy plays a critical role in 2D magnetic materials, and hence a generalized Heisenberg spin Hamiltonian model is established [3, 7, 41]. Bilayer $Cr_2Ge_2Te_6$ maintains long-range magnetic order at cryogenic temperatures and displays complex magnetic interactions with considerable magnetic anisotropy [42]. Intrinsic ferromagnetism and perpendicular magnetic anisotropy at room temperature in few-monolayer $CrTe_2$ films have been unambiguously evidenced by superconducting quantum interference and x-ray magnetic circular dichroism [43]. Sizable magnetic anisotropy energy and intrinsic antiferromagnetism have been discovered in 2D transition-metal borides [44]. By employing density functional theory calculations, 2D ferromagnetic rare-earth material $GdB_2N_2$ shows large perpendicular magnetic anisotropy at room temperature [45].

On the one hand, the edge effect on the magnetic and electronic properties of the layered 2D magnetic material is very significant [46–49]. For zigzag- or armchair-edged structures, the single-layer 2D MnO crystal has a degenerate antiferromagnetic ground state and a relatively less favorable ferromagnetic state [50]. $Ta_2S_3$ possesses a large out-of-plane magnetic anisotropy energy and high Curie temperature, and especially as the spin and orbital degrees of freedom couple, the $Ta_2S_3$ monolayer becomes a Chern insulator with a fully spin-polarized half-metallic edge state [51]. A new class of nonreciprocal edge spin waves exists in 2D antiferromagnetic nanoribbons [52]. On the other hand, controlling the magnetism of 2D magnetic materials by purely electrical means is also important, contributing to the development of information technology. The magnetic ground state of 2D antiferromagnet CrSBr bilayers [53] and $CrI_3$ bilayers [54–56] can be switched from antiferromagnetic to ferromagnetic with electric field. Electric-field-controlled magnetic phase transitions are achieved in the metamagnetic intermetallic alloy FeRh [57].

The surface anisotropy layer, to a certain degree, can influence the magnetization behavior of semi-infinite ferromagnets or thick films. However, the surface effect is very weak in the system, which is masked by the intrinsic bulk magnetic order [58, 59]. The properties of nanostructure Ising or Ising–Heisenberg spin systems are obviously changed when the edge of the system is modified [47, 60–62]. Half-metallicity in nanometer-scale graphene ribbons and scaling rules for the band gaps of graphene nanoribbons as a function of their widths are predicted by using first-principles calculations [63, 64]. Zigzag graphene nanoribbons exhibit the presence of nonbonding edge states that were predicted to realize a peculiar type of magnetic ordering [65, 66]. Magnetic zigzag edges of graphene exist despite the fact that no true long-range magnetic order is possible in one dimension [67, 68]. When one or both sides of the isotropic Heisenberg spin nanoribbon are modified with anisotropic spins, the system, whether or not long-range magnetic order is established, is worthy of further study. Therefore, we theoretically investigate Heisenberg spin nanoribbons decorated by magnetic anisotropy of side edge spins. The magnetic order and transition temperature of the system show some phenomena. The arrangement of the manuscript is as follows. In section 2, we will introduce the model and spin Green's function method in detail [69–72]. In section 3, the long-range magnetic order and transition temperature of the system are analyzed and discussed. Finally, a brief conclusion is given in section 4.

## 2. Model and method

In this paper, the magnetic order of nanoribbons with decoration on one side or two sides are investigated by use of the spin Green's function method. The schematic geometry of the system is depicted in figure 1, in which the blue and black balls denote two different Heisenberg spins with the spin quantum number $\boldsymbol{\mu} = 1$ and $\boldsymbol{S} = 1/2$ respectively. The structure is effectively infinite in the $y$ direction and has a finite width in the $x$ direction, where the lines of spins are labeled by an integer $n$ (= 1, 2, 3, ⋯, $N$).

The system is described by a Heisenberg model, and its Hamiltonian is written as,

$$H = -2J_s\sum_{\langle ij\rangle}\boldsymbol{\mu}_i\cdot\boldsymbol{\mu}_j - 2J_\perp\sum_{\langle ij\rangle}\boldsymbol{\mu}_i\cdot\boldsymbol{S}_j - 2J\sum_{\langle ij\rangle}\boldsymbol{S}_i\cdot\boldsymbol{S}_j - D\sum_i(\mu_i^z)^2, \quad (1)$$

where the index $\langle ij\rangle$ represents a pair of nearest-neighbor spins. The first three terms represent exchange interaction energies of the system, and $J_s$, $J_\perp$ and $J$ denote the exchange interaction between nearest-neighbor spins $\boldsymbol{\mu}$ and $\boldsymbol{\mu}$, $\boldsymbol{\mu}$ and $\boldsymbol{S}$, and $\boldsymbol{S}$ and $\boldsymbol{S}$ respectively. The last term presents the single-ion anisotropy energy of spin $\boldsymbol{\mu}$ in the system, and $D$ is the single-ion anisotropy parameter of spin $\boldsymbol{\mu}$. The retarded Green's function is introduced [71],

$$G_{ij}^{\epsilon_j}(t-t') = \langle\langle \epsilon_i^+(t); B_j^{\epsilon_j}(t')\rangle\rangle \quad (2)$$

where $B_j^{\epsilon_j} = e(\alpha^{\epsilon_j}\epsilon_j^z)\epsilon_j^-$, the spin raising and lowering operators of spin $\epsilon$ are defined as $\epsilon_i^\pm = \epsilon_i^x \pm i\epsilon_i^y$, and $\alpha^{\epsilon_i}$ is Callen's parameter [73], $\epsilon_i = \boldsymbol{S}_i$ or $\boldsymbol{\mu}_i$ dependent on the site

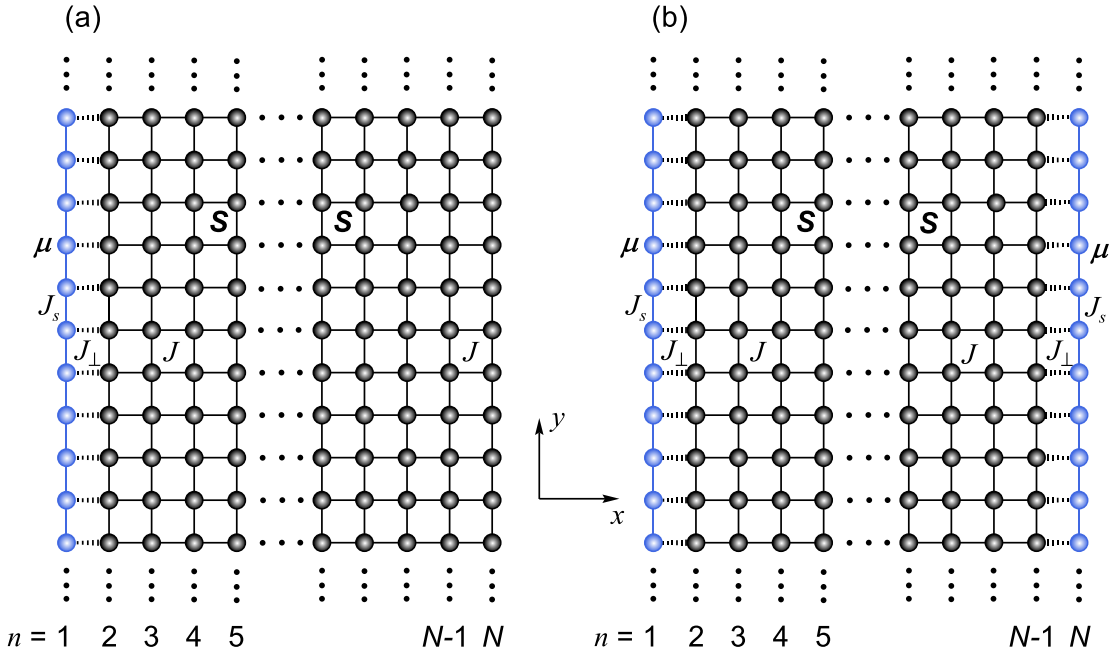


**Figure 1.** Schematic representations of (a) the nanoribbon with one side edge decoration and (b) the nanoribbon with double side edge decoration.

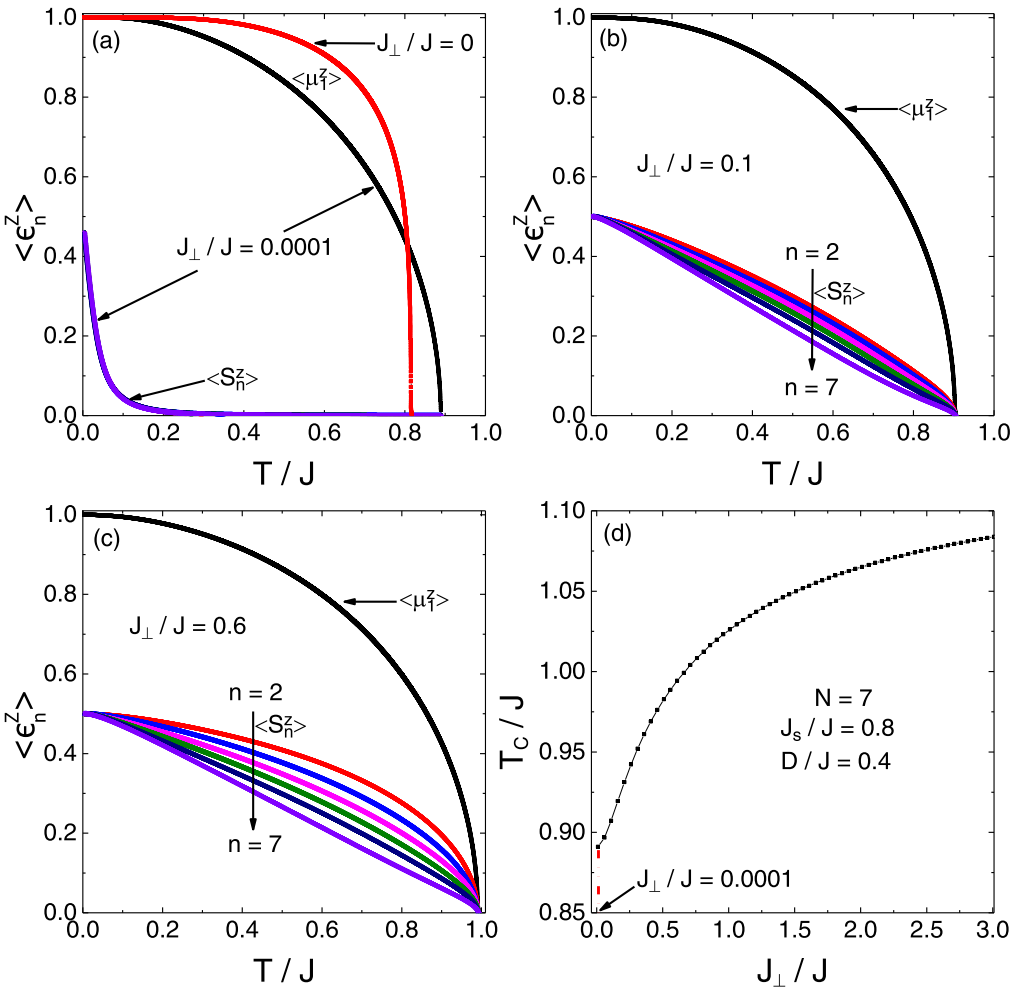


**Figure 2.** Temperature dependence of the magnetization of the nanoribbon with one side edge decoration for different coupling strengths between decorated spin and the nanoribbon with $N = 7$, $J_S/J = 0.8$, $D/J = 0.4$, for (a) $J_\perp/J = 0$ and $J_\perp/J = 0.0001$, (b) $J_\perp/J = 0.1$ and (c) $J_\perp/J = 0.6$, and (d) transition temperature $T_C/J$ versus $J_\perp/J$.

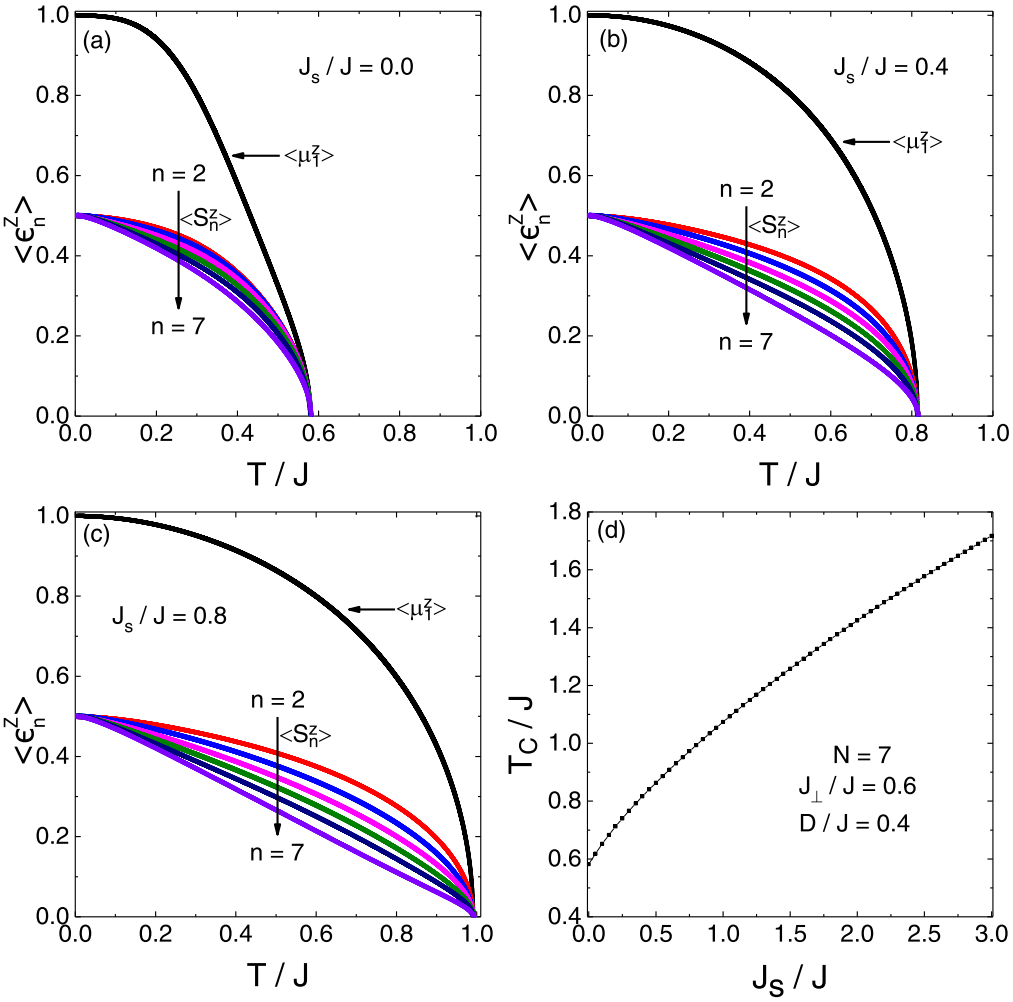


**Figure 3.** Temperature dependence of the magnetization of the nanoribbon with one side edge decoration for different coupling strengths between decorated spins with $N = 7$, $J_\perp/J = 0.6$, $D/J = 0.4$, for (a) $J_S/J = 0.0$, (b) $J_S/J = 0.4$ and (c) $J_S/J = 0.8$, and (d) transition temperature $T_C/J$ versus $J_s/J$.

position of $i$. Using time Fourier transforms and the equation of motion for Green's functions,

$$\omega\langle\langle A;B\rangle\rangle_\omega = \langle[A,\,B]\rangle\delta_{ij} + \langle\langle[A,\,H];B\rangle\rangle_\omega, \tag{3}$$

where $A$ and $B$ are two arbitrary operators respectively. For the transverse spin operator at site $i$ little correlated with the longitudinal spin operator at site $j$ ($i \neq j$), the higher order Green's function can be decoupled by the random-phase approximation [74],

$$\langle\langle \epsilon_i^z \epsilon_i^+;\, B_j^\epsilon\rangle\rangle \cong \langle\epsilon_i^z\rangle\langle\langle\epsilon_i^+;\, B_j^\epsilon\rangle\rangle. \tag{4}$$

Using Anderson–Callen decomposition [75], the higher order Green's function generated by single-ion anisotropy at the same lattice site can be expressed as,

$$\langle\langle(\mu_i^z\mu_i^+ + \mu_i^+\mu_i^z);\, B_j^\mu\rangle\rangle \approx 2\langle\mu_i^z\rangle\Theta_i\langle\langle\mu_i^+;\, B_j^\mu\rangle\rangle \tag{5}$$

where $\Theta_i = 1 - \frac{1}{2\mu^2}[\mu(\mu+1) - \langle\mu_i^z\mu_i^z\rangle]$.

By using spatial Fourier transforms [76, 77], we can obtain a group of equations about the Fourier component of the Green's function

$$(\omega\boldsymbol{I} - \boldsymbol{W})\boldsymbol{G} = \boldsymbol{F} \tag{6}$$

where $\boldsymbol{I}$ is the unit matrix. $\boldsymbol{F}$ is a one-dimensional column matrix,

$$\boldsymbol{F} = \begin{bmatrix} 2\langle\mu_1^z\rangle\delta_{1,n} \\ 2\langle S_2^z\rangle\delta_{2,n} \\ \vdots \\ 2\langle S_{N-1}^z\rangle\delta_{N-1,n} \\ 2\langle\epsilon_N^z\rangle\delta_{N,n} \end{bmatrix} \tag{7}$$

where the index 1, ⋯, $N$ denotes the order of the lines of spins, and the spatial Fourier component $\boldsymbol{G}$ in the $y$ direction of the Green's function is

$$\boldsymbol{G} = \begin{bmatrix} G_{1,n}^\mu \\ G_{2,n}^s \\ \vdots \\ G_{N-1,n}^s \\ G_{N,n}^\epsilon \end{bmatrix}. \tag{8}$$

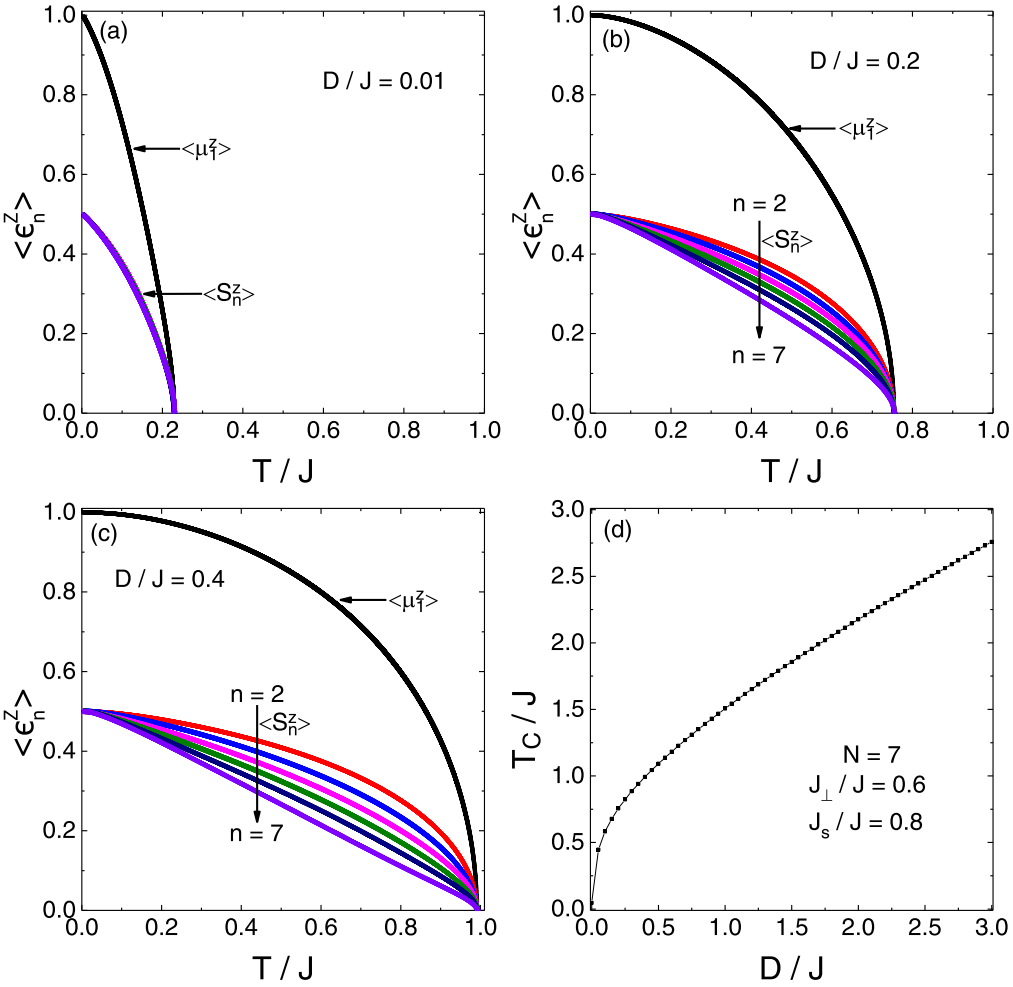


**Figure 4.** Temperature dependence of the magnetization of the nanoribbon with one side edge decoration for different coupling strengths between decorated spins with $N = 7$, $J_\perp/J = 0.6$, $J_S/J = 0.8$, for (a) $D/J = 0.01$, (b) $D/J = 0.2$ and (c) $D/J = 0.4$, and (d) transition temperature $T_C/J$ versus $D/J$.

The coefficient matrix $\boldsymbol{W}$ is expressed as

$$\boldsymbol{W} = \begin{bmatrix} X_1^{\mu} & -(p_1^{\mu})' & 0 & 0 & \cdots & 0 & 0 \\ -p_2^s & X_2^s & -(p_2^s)' & 0 & \cdots & 0 & 0 \\ 0 & -p_3^s & X_3^s & -(p_3^s)' & \cdots & 0 & 0 \\ \vdots & \vdots & \vdots & \vdots & \ddots & \vdots & \vdots \\ 0 & 0 & 0 & 0 & \cdots & X_{N-1}^s & -(p_{N-1}^s)' \\ 0 & 0 & 0 & 0 & \cdots & -p_N^{\epsilon} & X_N^{\epsilon} \end{bmatrix}. \tag{9}$$

When one side edge of the nanoribbon is decorated, the matrix elements of $\boldsymbol{W}$ are,

$$\begin{cases} X_1^{\mu} = 2J_s\langle\mu_1^z\rangle(z - z\gamma_{k_y}) + 2\langle\mu_1^z\rangle\Theta_1 D + 2J_\perp\langle S_2^z\rangle, \; n = 1 \\ X_2^s = 2J_\perp\langle\mu_1^z\rangle + 2J\langle S_2^z\rangle(z - z\gamma_{k_y}) + 2J\langle S_3^z\rangle, \; n = 2 \\ X_n^s = 2J\langle S_{n-2}^z\rangle + 2J\langle S_{n-1}^z\rangle(z - z\gamma_{k_y}) + 2J\langle S_n^z\rangle, \; 3 \leqslant n \leqslant N-1 \\ X_N^s = 2J\langle S_{N-1}^z\rangle + 2J\langle S_N^z\rangle(z - z\gamma_{k_y}), \; n = N \end{cases} \tag{10}$$

$$\begin{cases} p_2^s = 2J_\perp\langle S_2^z\rangle, \; n = 2 \\ p_n^s = 2J\langle S_n^z\rangle, \; 3 \leqslant n \leqslant N \\ (p_1^{\mu})' = 2J_\perp\langle\mu_1^z\rangle, \; n = 1 \\ (p_n^s)' = 2J\langle S_n^z\rangle, \; 2 \leqslant n \leqslant N-1 \end{cases}. \tag{11}$$

When both side edges of the nanoribbon are decorated, the four nonzero elements in the last two rows of the matrix $\mathbf{W}$ are replaced by

$$\begin{cases} X_{N-1}^s = 2JS_{N-2}^z + 2JS_{N-1}^z(z - z\gamma_{k_y}) + 2J_\perp\mu_N^z, \; n = N-1 \\ X_N^{\mu} = 2J_\perp S_{N-1}^z + 2J_s\mu_N^z(z - z\gamma_{k_y}) + 2\mu_N^z\Theta_N D, \; n = N \end{cases} \tag{12}$$

$$\begin{cases} (p_{N-1}^s)' = 2J_\perp\langle S_n^z\rangle, \; n = N-1 \\ p_N^{\mu} = 2J_\perp\langle\mu_N^z\rangle, \; n = N \end{cases} \tag{13}$$

where $z = 2$ and $\gamma_{k_y} = \cos(k_y)$, $k_y$ representing the wave vector in the $y$ axial direction within the first Brillouin zone. By means of the spectral theorem and Callen's technique [73], the magnetization of the $n$th line can be written as,

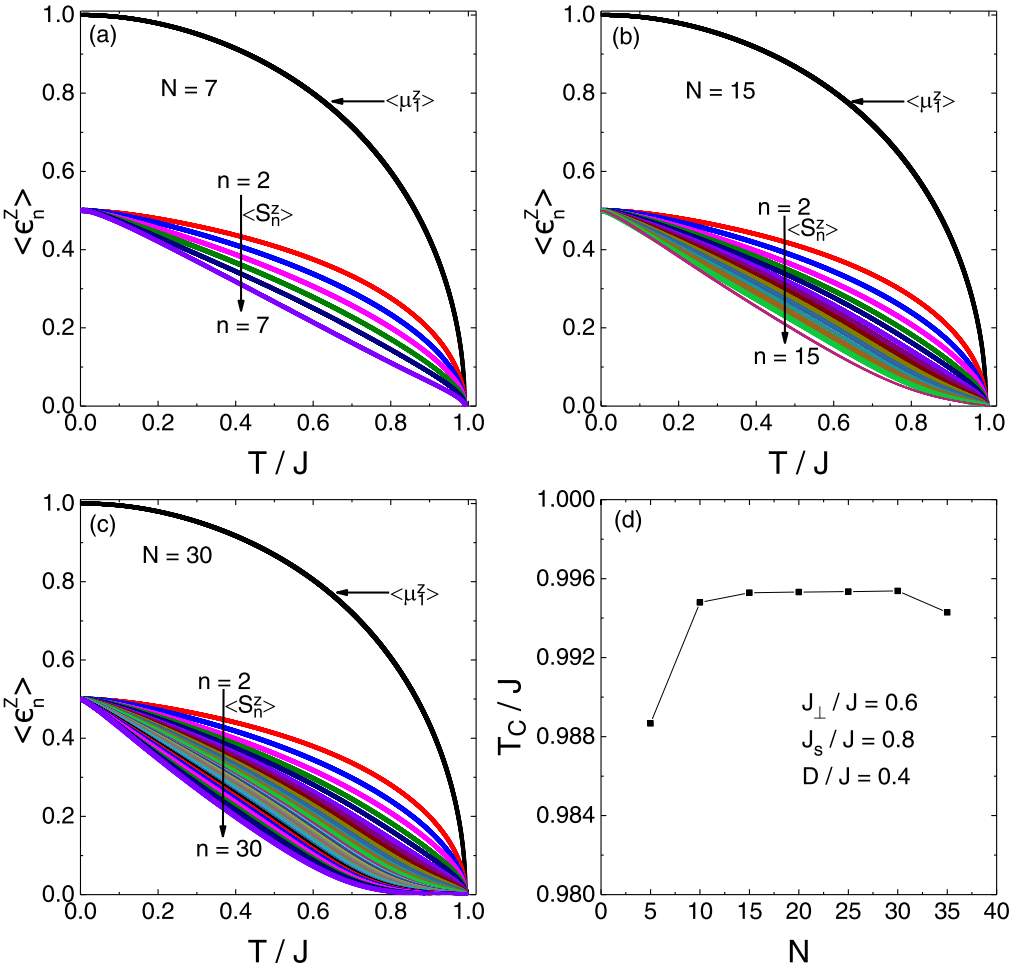


**Figure 5.** Temperature dependence of the magnetization of the nanoribbon with one side edge decoration for different widths of the nanoribbon with $D/J$=0.4, $J_\perp/J = 0.6$ and $J_S/J = 0.8$, for (a) $N = 7$, (b) $N = 15$ and (c) $N = 30$, and (d) transition temperature $T_C/J$ versus $N$.

$$\langle \epsilon_n^z \rangle = \frac{(\Phi_n + 1 + \epsilon_n)\Phi_n^{2\epsilon_n+1} - (\Phi_n - \epsilon_n)(\Phi_n + 1)^{2\epsilon_n+1}}{(\Phi_n + 1)^{2\epsilon_n+1} - \Phi_n^{2\epsilon_n+1}} \tag{14}$$

and the spin correlation function $\langle \epsilon_n^z \epsilon_n^z \rangle$, is given by,

$$\langle \epsilon_n^z \epsilon_n^z \rangle = \epsilon_n(\epsilon_n + 1) - (1 + 2\Phi_n)\langle \epsilon_n^z \rangle, \tag{15}$$

where $\epsilon_n$ denotes the spin quantum number of the spin in the $n$th line. The auxiliary function is written as,

$$\Phi_n = \frac{1}{N_y}\sum_{k_y}\sum_{i=1}^{N} \frac{R_{n,n}(\omega_i(k_y))}{(\mathrm{e}^{\beta\omega_i(k_y)} - 1)\prod_{j=1(j\neq i)}^{N}(\omega_i(k_y) - \omega_j(k_y))}, \tag{16}$$

where $\beta = 1/(k_B T)$, $k_y = \frac{2\pi m}{N_y a}$, $a$ is the lattice constant and the integer $m$ takes $-\frac{N_y}{2} < m \leqslant \frac{N_y}{2}$. $N_y$ denotes the number of the spin in a period in an infinite spin line. As $N_y$ is infinity, the summation of $k_y$ in equation (16) can be converted into the integral, namely $\frac{1}{N_y}\sum_{k_y} \to \frac{1}{2\pi}\int_{-\pi/a}^{\pi/a} \mathrm{d}k_y$. $R_{n,n}$ is the algebraic cofactor of element in matrix $\omega \boldsymbol{I} - \boldsymbol{W}$. The values of $\omega_i(k_y)$ define the spin wave spectrum which can be obtained from the coefficient matrix of equation (6). For convenience, $J_S$, $J_\perp$, $J$, $D$ and $T$ are reduced by $J$ ($J_S/J$, $J_\perp/J$, $D/J$ and $T/J$), $J = 1.0$ and $k_B = 1$.

## 3. Results and discussions

Firstly, we discuss the influence of the exchange interaction $J_\perp/J$ on the magnetization of the one side edge decorated nanoribbon, as shown in figures 2(a)–(c). For $J_S/J = 0.8$, $D/J = 0.4$ and $N = 7$, the transition temperature $T_C/J$ of the system is enhanced with increasing exchange interaction $J_\perp/J$. For the quasi-2D isotropic Heisenberg spin system, the system has a finite phase transition temperature when a very weak interaction is exhibited between two layers [78]. A similar phenomenon is also observed for the isotropic Heisenberg nanoribbon decorated by side spins with single-ion anisotropy. In figure 2(a), when the nanoribbon is not decorated ($J_\perp/J = 0$), the red line represents the behavior of the magnetization $\langle \mu^z \rangle$ with increasing temperature, and the phase transition temperature $T_C/J$ is about 0.81, but $\langle S^z \rangle = 0$. When $J_\perp/J = 0.0001$, the black line indicates the change of $\langle \mu^z \rangle$ with increasing temperature, and the magnetization $\langle S^z \rangle$ decreases faster and then forms a trail with increasing

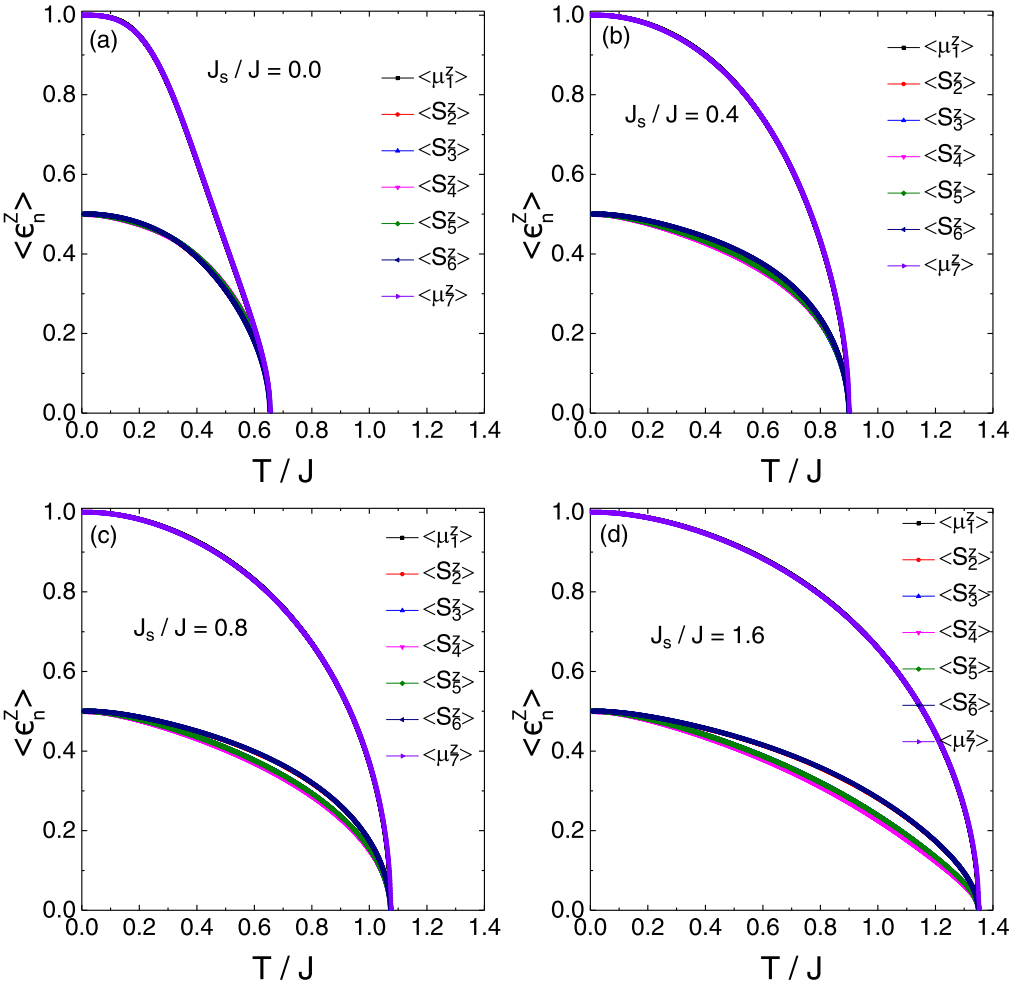


**Figure 6.** Temperature dependence of the magnetization of the nanoribbon with double side edge decoration for different coupling strengths between decorated spins with $N = 7$, $J_\perp/J = 0.6$ and $D/J = 0.4$, for (a) $J_s/J = 0.0$, (b) $J_s/J = 0.4$, (c) $J_s/J = 0.8$ and (d) $J_s/J = 1.6$.

temperature. The phase transition temperature $T_C/J$ of the nanoribbon is about 0.89. Compared with the red line, the black line decreases faster with the increase of temperature but has a larger transition temperature. As $J_\perp/J \neq 0$, the coordination number of the edge decorated spin increases, where the spin of the edge decorated chain affects the magnetic order of the nanoribbon, resulting in a faster decline of the magnetization of the edge decorated spin. And the magnetic order of the nanoribbon in turn influences the magnetic order of the edge decorated spin, which leads to a larger phase transition temperature of the edge decorated spin. The result means that spontaneous magnetization of the nanoribbon will disappear, once no exchange interaction exists between the host spins and the decorated edge spins. The magnetic order of the system is extraordinarily sensitive to the decorated edge spins. The magnetic order of the nanoribbon shows immediately as $J_\perp/J$ increases from 0 to 0.0001 in figure 2(a). Below the phase transition temperature, the magnetization of the lines of spins away from the decorated edge decreases in figures 2(b)–(c), which shows that the influence of the decorated edge on the magnetic order of the system decreases gradually with increasing distance from the decorated edge. The transition temperature $T_C/J$ of the system increases rapidly from a certain value, and then slowly with strengthening $J_\perp/J$ in figure 2(d) (the parameter $J_\perp/J$ starts from 0.0001). The certain value is the transition temperature of the decorated edge spins. For comparison, the transition temperatures of a 2D square lattice and simple cubic lattice are given respectively [73, 79].

The effect of the exchange interaction $J_S/J$ on the magnetization of the one side edge decorated nanoribbon is shown in figures 3(a)–(c). With $J_\perp/J = 0.6$, $D/J = 0.4$ and $N = 7$, the transition temperature $T_C/J$ of the system strengthens as the exchange interaction $J_S/J$ increases from zero in figure 3(d). A remarkable case is that, as the side edge decorated spins separate from each other ($J_S/J = 0.0$), the long-range magnetic order of the system still exists at nonzero temperature, as shown in figure 3(a). The system possesses spontaneous magnetization, whether the side edge decorated spins link together or separate from each other, even when they are arranged randomly.

The effect of the single-ion anisotropy $D/J$ on the magnetization of the one side edge decorated nanoribbon is shown in figures 4(a)–(c). With $J_\perp/J = 0.6$, $J_S/J = 0.8$ and $N = 7$, the transition temperature $T_C/J$ of the system strengthens rapidly from zero as $D/J$ increases from zero in figure 4(d). In

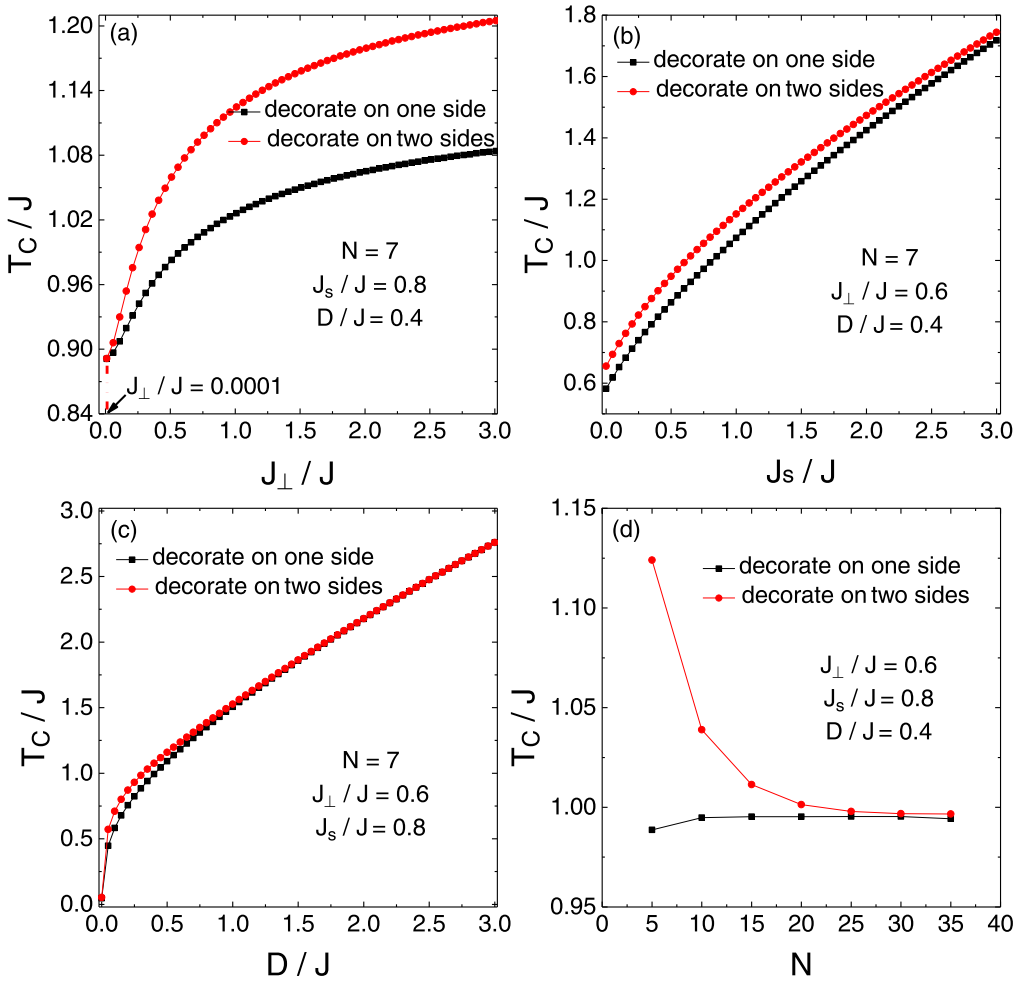


**Figure 7.** Transition temperature $T_C/J$ versus $J_\perp/J$ (a), $J_s/J$ (b), $D/J$ (c) and $N$ (d) respectively, (a) for $N = 7$, $D/J = 0.4$ and $J_s/J = 0.8$, (b) for $N = 7$, $D/J = 0.4$ and $J_\perp/J = 0.6$, (c) for $N = 7$, $J_s/J = 0.4$ and $J_\perp/J = 0.6$ and (d) for $J_s/J$=0.8, $D/J = 0.4$ and $J_\perp/J = 0.6$.

particular, when $D/J = 0.0$, no spontaneous magnetization in the system appears at nonzero temperature, as shown in figure 4(a), which abides by the Mermin–Wagner theorem [39]. The nonzero-temperature magnetic order of the system emerges immediately as existing magnetic anisotropy in the system, which is also consistent with Hohenberg's study [40]. These theoretical results can provide a comprehensive understanding of electric-field-induced magnetic phases in 2D van der Waals magnetic materials [53–57] and explain well the magnetism in graphene nanoribbons with zigzag edge [61, 80].

In figure 5, with $D/J = 0.4$, $J_\perp/J = 0.6$ and $J_S/J = 0.8$, the influence of the number of lines of spins $N$ (width of the nanoribbon) on the magnetization of the one side edge decorated nanoribbon is shown. The magnetization of the lines of spins, away from the decorated edge, obviously decreases faster and then forms a trail with increasing temperature. For $N < 10$, the transition temperature $T_C/J$ of the system enhances slowly with increasing width of the system, as shown in figure 5(d). However, when the number of lines of spins $N \geqslant 10$, the transition temperature $T_C/J$ of the system hardly changes as the width of the system increases. It can be inferred that, as the width of the nanoribbon approaches infinite limit $N\to\infty$, the nanoribbon becomes a semi-infinite 2D spin system and still maintains the same stable magnetic order. The results are quite different from those of the multilayer ferromagnetic films, where the influence of surface anisotropy on the long-range magnetic order in multilayer ferromagnetic films decreases with increasing film thickness, until the magnetic order is hidden by the intrinsic bulk magnetic order in multilayer ferromagnetic films [58, 59].

For a comprehensive understanding of the influence of various decorated edges on the nanoribbon, the double side edge decorated nanoribbon is also investigated. In figure 6, with $J_\perp/J = 0.6$, $D/J = 0.4$ and $N = 7$, the transition temperature $T_C/J$ of the system is enhanced as the exchange interaction $J_S/J$ increases from zero, which is similar to the result for the one side edge decorated nanoribbon. According to two-fold symmetry of the system (shown in figure 1(b)), the magnetization of the system shows four temperature behaviors, $\langle\mu_1^z\rangle$=$\langle\mu_7^z\rangle$, $\langle S_2^z\rangle$=$\langle S_6^z\rangle$, $\langle S_3^z\rangle$=$\langle S_5^z\rangle$ and $\langle S_4^z\rangle$ respectively. The middle line of spins, away from the decorated edge, shows the smallest magnetization.

The transition temperatures influenced by $J_\perp/J$, $J_s/J$, $D/J$ and $N$ are investigated both in the one side edge decorated nanoribbon and the double side edges decorated nanoribbon. In figure 7(a), with $N = 7$, $D/J = 0.4$ and $J_s/J = 0.8$, the transition temperature of the double side edges decorated

nanoribbon increases faster and eventually achieves a larger value with increasing $J_\perp/J$ than that of the one side edge decorated nanoribbon. In figure 7(b), with $N = 7$, $D/J = 0.4$ and $J_\perp/J = 0.6$, and increasing $J_s/J$, the transition temperature of the one side edge decorated nanoribbon approaches gradually that of the double side edges decorated nanoribbon. In figure 7(c), with $N = 7$, $J_s/J = 0.8$ and $J_\perp/J = 0.6$, an unexpected phenomenon is found in that the behaviors of transition temperature are almost the same with increasing $D/J$ in both the one side edge decorated nanoribbon and the double side edges decorated nanoribbon. In figure 7(d), with $D/J = 0.4$, $J_s/J = 0.8$ and $J_\perp/J = 0.6$, when the number of lines of spins $N$ increases, the transition temperature of the one side edge decorated nanoribbon increases very slowly and then tends to a constant value, but the transition temperature of the double side edge decorated nanoribbon decreases and then tends to the same constant value. The results reveal that, as $N\to\infty$, the long-range magnetic orders are similar both in the one side edge decorated nanoribbon and the double side edge decorated nanoribbon.

## 4. Conclusion

For the one side edge decorated and double side edge decorated Heisenberg spin nanoribbons, five main cases are summarized: (I) the transition temperature of the system is enhanced by increasing the exchange interaction $J_\perp/J$ between the host spins and decorated edge spins. In particular, no long-range magnetic order appears in the system (excluding decorated edge spins) at nonzero temperature when $J_\perp/J = 0$. (II) A remarkable case is that, as the decorated edge spins separate from each other, the long-range magnetic order of the system still exists at nonzero temperature. The system possesses spontaneous magnetization, whether the decorated side edge spins link together or separate from each other, even when they are arranged randomly. (III) The transition temperature of the system strengthens rapidly from zero with single-ion anisotropy $D/J$ increasing from zero. In particular, when $D/J = 0$, no magnetic order of the system appears at nonzero temperature. (IV) Below phase transition temperature, the magnetization of the lines of spins away from the decorated side edge decreases, which illustrates that the influence of the decorated edge on the magnetic order of the system decreases gradually with increasing distance from the decorated edge. (V) When the number of lines of spins $N$ increases, the transition temperature of the one side edge decorated nanoribbon increases very slowly and then tends to a constant value, but the transition temperature of the double side edge decorated nanoribbon decreases and then tends to the same constant value. In particular, as $N\to\infty$, the long-range magnetic orders are similar both in the one side edge decorated nanoribbon and the double side edge decorated nanoribbon.

## Acknowledgments

This paper is supported by the 111 Project (B16009).

## References

[1] Burch K S, Mandrus D and Park J G 2018 Magnetism in two-dimensional van der Waals materials *Nature* **563** 47–52
[2] Samarth N 2017 Magnetism in flatland *Nature* **546** 216–7
[3] Gong C *et al* 2017 Discovery of intrinsic ferromagnetism in two-dimensional van der Waals crystals *Nature* **546** 265–9
[4] Huang B *et al* 2017 Layer-dependent ferromagnetism in a van der Waals crystal down to the monolayer limit *Nature* **546** 270–3
[5] Lin M-W *et al* 2016 Ultrathin nanosheets of CrSiTe3: a semiconducting two-dimensional ferromagnetic material *J. Mater. Chem.* C **4** 315–22
[6] Du K Z, Wang X Z, Liu Y, Hu P, Utama M I, Gan C K, Xiong Q and Kloc C 2016 Weak van der Waals stacking, wide-range band gap, and Raman study on ultrathin layers of metal phosphorus trichalcogenides *ACS Nano* **10** 1738–43
[7] Gibertini M, Koperski M, Morpurgo A F and Novoselov K S 2019 Magnetic 2D materials and heterostructures *Nat. Nanotechnol.* **14** 408–19
[8] Xian J-J *et al* 2022 Spin mapping of intralayer antiferromagnetism and field-induced spin reorientation in monolayer $CrTe_2$ *Nat. Commun.* **13** 257
[9] González-García A, López-Pérez W, González-Hernández R, Bacaksiz C, Šabani D, Milošević M V and Peeters F M 2021 Transition-metal adatoms on 2D-GaAs: a route to chiral magnetic 2D materials by design *J. Phys.: Condens. Matter* **33** 145803
[10] Saritas K and Ismail-Beigi S 2022 Piezoelectric ferromagnetism in two-dimensional materials via materials screening *Phys. Rev.* B **106** 134421
[11] Hua C-B, Xiao F, Liu Z-R, Sun J-H, Gao J-H, Chen C-Z, Tong Q, Zhou B and Xu D-H 2023 Magnon corner states in twisted bilayer honeycomb magnets *Phys. Rev.*B **107** L020404
[12] Park M J, Jeon S, Lee S, Park H C and Kim Y 2021 Higher-order topological corner state tunneling in twisted bilayer graphene *Carbon* **174** 260–5
[13] Sun Q, Ma Y and Kioussis N 2020 Two-dimensional Dirac spin-gapless semiconductors with tunable perpendicular magnetic anisotropy and a robust quantum anomalous Hall effect *Mater. Horiz.* **7** 2071–7
[14] Zhou J, Song X, Yang M, Chai J, Wong N L M, Shen L, Wang S and Feng Y P 2021 A first principles study of uniaxial strain-stabilized long-range ferromagnetic ordering in electrenes *J. Mater. Chem.* C **9** 16576–80
[15] Kuo C T *et al* 2016 Exfoliation and Raman spectroscopic fingerprint of few-layer $NiPS_3$ van der Waals crystals *Sci. Rep.* **6** 20904
[16] Zhang B Y, Xu K, Yao Q, Jannat A, Ren G, Field M R, Wen X, Zhou C, Zavabeti A and Ou J Z 2021 Hexagonal metal oxide monolayers derived from the metal–gas interface *Nat. Mater.* **20** 1073–8
[17] Novoselov K S, Geim A K, Morozov S V, Jiang D, Zhang Y, Dubonos S V, Grigorieva I V and Firsov A A 2004 Electric field effect in atomically thin carbon films *Science* **306** 666–9
[18] Kurebayashi H, Garcia J H, Khan S, Sinova J and Roche S 2022 Magnetism, symmetry and spin transport in van der Waals layered systems *Nat. Rev. Phys.* **4** 150–66
[19] Bedoya-Pinto A, Ji J-R, Pandeya A K, Gargiani P, Valvidares M, Sessi P, Taylor J M, Radu F, Chang K and

Parkin S S P 2021 Intrinsic 2D-XY ferromagnetism in a van der Waals monolayer *Science* **374** 616–20
[20] Wang H, Li X, Wen Y, Cheng R, Yin L, Liu C, Li Z and He J 2022 Two-dimensional ferromagnetic materials: from materials to devices *Appl. Phys. Lett.* **121** 220501
[21] Rizzo D J *et al* 2022 Visualizing atomically layered magnetism in CrSBr *Adv. Mater.* **34**
[22] Lasek K, Coelho P M, Gargiani P, Valvidares M, Mohseni K, Meyerheim H L, Kostanovskiy I, Zberecki K and Batzill M 2022 van der Waals epitaxy growth of 2D ferromagnetic $Cr(1+\delta)Te_2$ nanolayers with concentration-tunable magnetic anisotropy *Appl. Phys. Rev.* **9**
[23] Peng J *et al* 2023 Even–odd-layer-dependent ferromagnetism in 2D non-van-der-Waals $CrCuSe_2$ *Adv. Mater.* **35**
[24] Ji A-C, Liu W M, Song J L and Zhou F 2008 Dynamical creation of fractionalized vortices and vortex lattices *Phys. Rev. Lett.* **101**
[25] Ji A-C, Xie X C and Liu W M 2007 Quantum magnetic dynamics of polarized light in arrays of microcavities *Phys. Rev. Lett.* **99**
[26] Qi R, Yu X-L, Li Z B and Liu W M 2009 Non-abelian Josephson effect between two $F$=2 spinor Bose–Einstein condensates in double optical traps *Phys. Rev. Lett.* **102**
[27] Yun S, Shiping F and Benkun M 1999 Self-consistent mean-field theory of two-dimensional anisotropic Heisenberg antiferromagnet *Commun. Theor. Phys.* **31** 199
[28] Song T *et al* 2021 Direct visualization of magnetic domains and moiré magnetism in twisted 2D magnets *Science* **374** 1140–4
[29] Xu Y *et al* 2022 Coexisting ferromagnetic–antiferromagnetic state in twisted bilayer $CrI_3$ *Nat. Nanotechnol.* **17** 143–7
[30] Xie H *et al* 2021 Twist engineering of the two-dimensional magnetism in double bilayer chromium triiodide homostructures *Nat. Phys.* **18** 30–36
[31] Yang X, Zhou X, Feng W and Yao Y 2021 Tunable magneto-optical effect, anomalous Hall effect, and anomalous Nernst effect in the two-dimensional room-temperature ferromagnet 1T-$CrTe_2$ *Phys. Rev.* B **103**
[32] Freitas D C, Weht R, Sulpice A, Remenyi G, Strobel P, Gay F, Marcus J and Nunez-Regueiro M 2015 Ferromagnetism in layered metastable 1T-$CrTe_2$ *J. Phys.: Condens. Matter* **27** 176002
[33] Sun X *et al* 2020 Room temperature ferromagnetism in ultra-thin van der Waals crystals of 1T-$CrTe_2$ *Nano Res.* **13** 3358–63
[34] Purbawati A *et al* 2020 In-plane magnetic domains and Néel-like domain walls in thin flakes of the room temperature $CrTe_2$ van der Waals ferromagnet *ACS Appl. Mater. Interfaces* **12** 30702–10
[35] Fei Z *et al* 2018 Two-dimensional itinerant ferromagnetism in atomically thin $Fe_3GeTe_2$ *Nat. Mater.* **17** 778–82
[36] Zhang G, Guo F, Wu H, Wen X, Yang L, Jin W, Zhang W and Chang H 2022 Above-room-temperature strong intrinsic ferromagnetism in 2D van der Waals $Fe_3GaTe_2$ with large perpendicular magnetic anisotropy *Nat. Commun.* **13** 5067
[37] Wang X, Li D, Li Z, Wu C, Che C M, Chen G and Cui X 2021 Ferromagnetism in 2D vanadium diselenide *ACS Nano* **15** 16236–41
[38] Hovančík D, Pospíšil J, Carva K, Sechovský V and Piamonteze C 2023 Large orbital magnetic moment in $VI_3$ *Nano Lett.* **23** 1175–80
[39] Mermin N D and Wagner H 1966 Absence of ferromagnetism or antiferromagnetism in one- or two-dimensional isotropic Heisenberg models *Phys. Rev. Lett.* **17** 1133–6
[40] Hohenberg P C 1967 Existence of long-range order in one and two dimensions *Phys. Rev.* **158** 383–6
[41] Jiang X, Liu Q, Xing J, Liu N, Guo Y, Liu Z and Zhao J 2021 Recent progress on 2D magnets: fundamental mechanism, structural design and modification *Appl. Phys. Rev.* **8**
[42] Liu Y *et al* 2022 Polaronic conductivity in $Cr_2Ge_2Te_6$ single crystals *Adv. Funct. Mater.* **32** 2105111
[43] Zhang X *et al* 2021 Room-temperature intrinsic ferromagnetism in epitaxial $CrTe_2$ ultrathin films *Nat. Commun.* **12**
[44] Wang S, Miao N, Su K, Blatov V A and Wang J 2021 Discovery of intrinsic two-dimensional antiferromagnets from transition-metal borides *Nanoscale* **13** 8254–63
[45] Tan H, Shan G and Zhang J 2022 Prediction of novel two-dimensional room-temperature ferromagnetic rare-earth material—$GdB_2N_2$ with large perpendicular magnetic anisotropy *Mater. Today Phys.* **24** 100700
[46] Kunstmann J, Özdoğan C, Quandt A and Fehske H 2011 Stability of edge states and edge magnetism in graphene nanoribbons *Phys. Rev.* B **83** 045414
[47] Ma D-c and Du A 2023 The exact solution of the edge-modified graphene nanoribbon-like structure Ising–Heisenberg spin (1, 1/2) system *Physica*E **147** 115569
[48] Train C, Baudelet F and Cartier dit Moulin C 2004 Remnant x-ray magnetic circular dichroism investigation of the local magnetic contributions to the magnetization of a coercive bimetallic molecule-based magnet *J. Phys. Chem.* B **108** 12413–7
[49] Qiu G, Li Z, Zhou K and Cai Y 2023 Flexomagnetic noncollinear state with a plumb line shape spin configuration in edged two-dimensional magnetic $CrI_3$ *npj Quantum Mater.* **8** 1–6
[50] Sozen Y, Topkiran U C and Sahin H 2022 Magnetic single-layer nanoribbons of manganese oxide: edge- and width-dependent electronic properties *J. Mater. Chem.* C **10** 7567–74
[51] Zhang L, Zhang C-w, Zhang S-F, Ji W-x, Li P and Wang P-j 2019 Two-dimensional honeycomb-Kagome $Ta_2S_3$: a promising single-spin Dirac fermion and quantum anomalous Hall insulator with half-metallic edge states *Nanoscale* **11** 5666–73
[52] Ghader D and Khater A 2019 A new class of nonreciprocal spin waves on the edges of 2D antiferromagnetic honeycomb nanoribbons *Sci. Rep.* **9**
[53] Wang Y, Luo N, Zeng J, Tang L-M and Chen K-Q 2023 Magnetic anisotropy and electric field induced magnetic phase transition in the van der Waals antiferromagnet CrSBr *Phys. Rev.*B **108** 054401
[54] Xu R and Zou X 2020 Electric field-modulated magnetic phase transition in van der Waals $CrI_3$ bilayers *J. Phys. Chem. Lett.* **11** 3152–8
[55] Huang B *et al* 2018 Electrical control of 2D magnetism in bilayer $CrI_3$ *Nat. Nanotechnol.* **13** 544–8
[56] Jiang S, Shan J and Mak K F 2018 Electric-field switching of two-dimensional van der Waals magnets *Nat. Mater.* **17** 406–10
[57] Feng Z, Yan H and Liu Z 2018 Electric-field control of magnetic order: from FeRh to topological antiferromagnetic spintronics *Adv. Electron. Mater.* **5**
[58] Endo Y and Ayukawa T 1990 Magnetic properties of Heisenberg-type ferromagnetic films with a sandwich structure *Phys. Rev.*B **41** 6777–82
[59] Endo Y 1992 Magnetization direction of a semi-infinite Heisenberg ferromagnet with perpendicular surface anisotropy *Phys. Rev.*B **46** 11129–32
[60] Ma D-C, Chi X-D and Du A 2024 Natural pinning field effecting on one surface of $C_{60}$-like-nanostructure antiferromagnetic mixed-spin (1/2, 1) Ising spin system *Results Phys.* **56**

[61] Pizzochero M and Kaxiras E 2022 Hydrogen atoms on zigzag graphene nanoribbons: chemistry and magnetism meet at the edge *Nano Lett.* **22** 1922–8
[62] Ma D-C and Du A 2022 The exact solution of the edge-modified kekulene-like nanostructure Ising–Heisenberg spin system *Physica*E **144**
[63] Son Y W, Cohen M L and Louie S G 2006 Half-metallic graphene nanoribbons *Nature* **444** 347–9
[64] Son Y-W, Cohen M L and Louie S G 2006 Energy gaps in graphene nanoribbons *Phys. Rev. Lett.* **97**
[65] Fujita M, Wakabayashi K, Nakada K and Kusakabe K 1996 Peculiar localized state at zigzag graphite edge *J. Phys. Soc. Japan* **65** 1920–3
[66] Nakada K, Fujita M, Dresselhaus G and Dresselhaus M S 1996 Edge state in graphene ribbons: nanometer size effect and edge shape dependence *Phys. Rev.* B **54** 17954–61
[67] Yazyev O V and Katsnelson M I 2008 Magnetic correlations at graphene edges: basis for novel spintronics devices *Phys. Rev. Lett.* **100** 047209
[68] Yazyev O V 2010 Emergence of magnetism in graphene materials and nanostructures *Rep. Prog. Phys.* **73**
[69] Tyablikov S V 1967 *Methods in the Quantum Theory of Magnetism* (Plenum Press) 205–311
[70] Tahir-Kheli R A and ter Haar D 1962 Use of Green functions in the theory of ferromagnetism. I. General discussion of the spin-*S* case *Phys. Rev.* **127** 88–94
[71] Tyablikov S V 1959 Retarded and advanced Green functions in the theory of ferromagnetism *Ukr. Mat. Zh.* **11** 1318–1329
[72] XianYu Z-N and Du A 2018 Magnetic properties of XXZ Heisenberg antiferromagnetic and ferrimagnetic nanotubes *Commun. Theor. Phys.* **70**
[73] Callen H B 1963 Green function theory of ferromagnetism *Phys. Rev.* **130** 890–8
[74] Englert F 1960 Theory of a Heisenberg ferromagnet in the random phase approximation *Phys. Rev. Lett.* **5** 102–3
[75] Anderson F B and Callen H B 1964 Statistical mechanics and field-induced phase transitions of the Heisenberg antiferromagnet *Phys. Rev.* **136** A1068–87
[76] Mi B-Z, Wang H-Y and Zhou Y-S 2010 Theoretical investigations of magnetic properties of ferromagnetic single-walled nanotubes *J. Magn. Magn. Mater.* **322** 952–8
[77] XianYu Z-N and Du A 2019 Magnetization behavior of a single-walled nanotube ring with surface anisotropy *J. Magn. Magn. Mater.* **485** 265–70
[78] Guo-Zhu W, An D and Rong-ke Q 1996 Magnetization of layered Heisenberg ferrimagnets *J. Phys.: Condens. Matter* **8** 5039
[79] Reinehr E E and Figueiredo W 1995 Anisotropic Heisenberg ferromagnetic model in two dimensions *Phys. Rev.*B **52** 310–2
[80] Pizzochero M and Kaxiras E 2021 Imprinting tunable $\pi$-magnetism in graphene nanoribbons via edge extensions *J. Phys. Chem. Lett.* **12** 1214–9